

The functional environment of chondrocytes within cartilage subjected to compressive loading: A theoretical and experimental approach

Christopher C.-B. Wang, X. Edward Guo, Dongning Sun, Van C. Mow, Gerard A. Ateshian and Clark T. Hung*

Department of Biomedical Engineering, Columbia University, New York, NY 10027, USA

Abstract. A non-invasive methodology (based on video microscopy, optimized digital image correlation and thin plate spline smoothing technique) has been developed to determine the intrinsic tissue stiffness (H_a) and the intrinsic fixed charge density (c_0^F) distribution for hydrated soft tissues such as articular cartilage. Using this technique, the depth-dependent inhomogeneous parameters $H_a(z)$ and $c_0^F(z)$ were determined for young bovine cartilage and incorporated into a triphasic mixture model. This model was then used to predict the mechanical and electrochemical events (stress, strain, fluid/osmotic pressure, and electrical potentials) inside the tissue specimen under a confined compression stress relaxation test. The integration of experimental measurements with theoretical analyses can help to understand the unique material behaviors of articular cartilage. Coupled with biological assays of cell-scale biosynthesis, there is also a great potential in the future to study chondrocyte mechanotransduction *in situ* with a new level of specificity.

1. Introduction

A major motivation for cartilage biomechanics research has been to provide a greater insight into the interaction among the type II collagen meshwork, the fixed negative charges of the entrapped proteoglycan, and the ion-rich interstitial fluid that gives rise to the load-bearing capacity of this specialized connective tissue [24,29,32]. Consisting of 3–10% proteoglycans, 10–30% collagen, 60–80% water, the distribution of each component varies with the depth of the tissue. Although well recognized, the physiologic implications of this inhomogeneity on tissue function and chondrocyte activities remain to be elucidated. The study of cartilage inhomogeneity has been traditionally addressed by slicing the tissue into thin “homogenized” strips to be tested in uniaxial tension or compression [1,19,25,41,62].

There have been significant advances in cartilage mechanical testing by the introduction of various optical-based techniques [18,27,35,36,42,43,58,59]. Similarly, advances in constitutive modeling of hydrated soft tissues (e.g., [12,13,21,31,52]) have contributed to the understanding of cartilage structure-function relationship (Fig. 1). Motivated by these advances, we have developed an automated approach for determination of the intrinsic tissue properties (e.g., intrinsic solid matrix stiffness and intrinsic fixed

* Address for correspondence: Dr. Clark T. Hung, Cellular Engineering Laboratory, Department of Biomedical Engineering, Columbia University, 3513 Engineering Terrace, M.C. 8904, 1210 Amsterdam Avenue, New York, NY 10027, USA. Tel.: +1 212 854 6542; Fax: +1 212 854 8725; E-mail: cth6@columbia.edu.

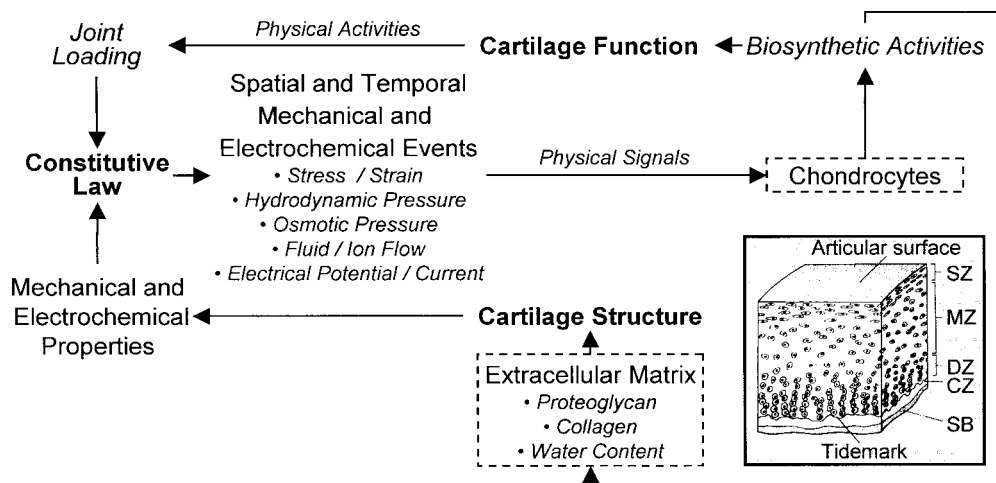


Fig. 1. A schematic of the structure–function relationship of articular cartilage. The extracellular matrix, with associated interstitial fluid, solutes and ions, can collectively be thought of as a mechanical signal transducer that receives mechanical input in the form of joint or explant loading and yields an output of various extracellular signals.

charge density (FCD)) of full-thickness cartilage explants using a combination of applied osmotic chemical loading and mechanical loading. With the knowledge gained from this technique, we are in a position to provide a more refined description of the chondrocyte environment (e.g., hydrostatic pressure, deformation, fluid, electrokinetic, and osmotic pressure fields) *in situ*.

Through these efforts, we can better identify the stimuli and their appropriate levels that the cells may see *in situ*. New information regarding the *in situ* environment of the cell will provide motivation for *in vitro* cell and explant studies to study physical effects on chondrocytes, whose metabolic and catabolic activities regulate cartilage maintenance. The role of a particular stimulus can then be identified using *in vitro* models aimed at simplifying the cell environment or delineating the role of concomitant stimuli [5,7,15,17,22,23,28,37,39,47,48]. Thus, the application of constitutive modeling permits an understanding of the potential contributions of specific stimuli that cannot be directly inferred from experiments alone.

We have previously [56,57] described the effect of an inhomogeneous aggregate modulus on the stress relaxation response of a cartilage explant using a biphasic analysis [31]. In this earlier study, the depth-dependent distribution of tissue stiffness was obtained from the work of Schinagl and co-workers [42,43] using digital video microscopy and fluorescently labeled cell nuclei as fiducial markers. Additionally, we have also considered the effect of an inhomogeneous FCD on the mechano-electrochemical behavior of cartilage [53] using the triphasic mechano-electrochemical theory which considers the tissue as consisting of solid, fluid and ion phases [21]. The depth-dependent FCD distribution for this analysis was based on the depth-dependent variation of FCD reported in the literature [25]. In the current study, we describe our approach to integrating novel experimental measurements of depth-varying intrinsic tissue stiffness and intrinsic FCD [55] with the triphasic theory to describe the chondrocyte environment within articular cartilage during the stress relaxation response of a tissue explant subjected to loading in confined compression.

2. Methods

2.1. Triphasic mixture model for articular cartilage

In the triphasic mixture theory, the articular cartilage is modeled as a composite material with three interacting incompressible phases: (1) a charged solid phase, which is composed predominately of a densely-woven, strong, collagen fibrillar network enmeshed with a high concentration of charged proteoglycan aggregates; (2) an interstitial fluid phase which is water; and (3) an ion phase of both cation and anion species, which is required to neutralize the charges fixed to the collagen–proteoglycan solid matrix. According to this theory,

1. The net charge at every point within the tissue is zero. This assumption, i.e., the electroneutrality condition, can be expressed in terms of ion concentrations and valance by:

$$\sum_{\alpha} z_{\alpha} c_{\alpha} - c^F = 0,$$

where z_{α} is the valance of the α th ionic species including sign (+/−), c_{α} (mol/m³) is the molar concentration of the α th ionic species (per unit of solvent volume) and c^F (mEq/ml) is the effective FCD of the tissue. The effective FCD is related to the intrinsic FCD (c_0^F) by the conservation equation of fixed charges:

$$c^F = \frac{c_0^F}{1 + \varepsilon/\phi_0^w}, \quad (1)$$

where ϕ_0^w is the intrinsic porosity of the tissue¹.

2. The only motive forces for interstitial fluid flow and ion transport are the gradients of their electrochemical potentials; and
3. Frictional forces exist when there is relative motion between these three phases of the tissue; however, the frictional force between the solid matrix and the ions are negligible.

In this triphasic theory, the total stress σ^T may be decomposed into partial stresses, an elastic stress σ_E^s and the fluid pressure p (which includes the osmotic pressure):

$$\sigma^T = \sigma_E^s - p\mathbf{I}. \quad (2)$$

At equilibrium, the fluid pressure $p = \pi$ is the Donnan osmotic pressure given by van't Hoff pressure law:

$$\pi = RT \left(\sum_{\alpha} (\phi_{\alpha} c_{\alpha}) - \sum_{\alpha} (\phi_{\alpha}^* c_{\alpha}^*) \right), \quad (3)$$

where R is the universal gas constant, T is the absolute temperature, and ϕ_{α} and ϕ_{α}^* are osmotic coefficients²; the superscript (*) denotes the quantities associated with the external solutions.

¹ ϕ_0^w is assumed constant through the depth of cartilage in this study.

²In the current study we assume $\phi_{\alpha} \approx \phi_{\alpha}^* \approx 1$.

The electrochemical potentials of the ions within the interstitium of cartilage are given by:

$$\mu^\alpha = \mu_0^\alpha + \frac{RT}{M_\alpha} \ln(\gamma_\alpha c_\alpha) + z_\alpha \frac{F_c \psi}{M_\alpha}, \quad (4)$$

where μ_0^α are the reference potentials of the α th ionic species, γ_α are the activity coefficients of c_α , M_α are the atomic weight of these ions, F_c is the Faraday constant and ψ is the electric potential.

2.2. One-dimensional (1D) confined compression test

Normal articular cartilage is firmly attached to the impermeable subchondral bone, and articulates against an opposing cartilage surface. Thus one needs to examine how articular cartilage will respond when pressed against a solid material. In a 1D confined compression test, all motions are uniaxial in the direction of the applied load. This test requires a precisely prepared cartilage specimen harvested from an articular layer. The experiment calls for inserting this cartilage specimen into a frictionless, impermeable confining chamber (to prevent lateral expansion and fluid flow), and loading it axially between two rigid solid loading platens. The top platen is porous-permeable to permit the interstitial fluid and ions to flow out of the tissue. The pore pressure within this free-draining loading platen is ambient.

In this study, a stress–relaxation test is analyzed using the triphasic mixture theory to study the mechanical and electrochemical events of a tissue under confined compression. In such a test, the surface-to-surface strain ε_o (say 10%) is imposed in a linear manner over the time duration $0 < t < t_o$ (e.g., 400 seconds). For time $t > t_o$, the strain ε_o is maintained constant for the remainder of the experiment. Under this test configuration, the elastic stress (σ_E^s) is given by

$$\sigma_E^s = H_a \varepsilon, \quad (5)$$

where H_a is the intrinsic stiffness of the solid matrix at equilibrium and ε the strain inside the tissue.

In this 1D configuration, the general equations of the triphasic constitutive law are reduced to a system of partial differential equations with u (matrix displacement) and c^+ (cation concentration) as dependent variables, and z (depth) and t (time) as independent variables. The system of partial differential equations can be solved numerically by finite element or finite difference methods [34,53]. The intrinsic stiffness of the solid matrix (H_a) and the intrinsic FCD (c_0^F) are two of the most important parameters that govern the mechanical and electrochemical behavior of the tissue. Both H_a and c_0^F have been found to vary significantly through the depth (z -direction) of the tissue [25,42]. Consequently, these inhomogeneous material properties will lead to the development of non-uniform mechanical and electrochemical events ($\sigma(z, t)$, $\varepsilon(z, t)$, $\pi(z, t)$, etc.) during the transient phase of loading and at equilibrium. Below, we describe a methodology to determine these important parameters on the same tissue specimen without sectioning the specimen in the axial (or depth) direction.

2.3. Experimental measurement of cartilage properties

Healthy carpometacarpal joints from 1- to 2-month-old calves were obtained from a local slaughterhouse 6–10 hours post-mortem. A steel trephine with a 6mm diameter core was used to harvest cartilage-bone plugs with the core axis perpendicular to the articular surface. Following harvesting, the plugs were rinsed with phosphate buffered saline (PBS) containing protease inhibitors (PI) and frozen at -80°C for storage until the day of use. On the day of testing, plugs were thawed to room temperature by immersion

in freshly prepared PBS + PI solution. The plug was microtomed to remove residual subchondral bone and vascularized deep zone only, leaving the articular surface intact. 2 mm-diameter disks were cored out from each plug with a stainless-steel micro-dissecting trephine (Biomedical Research Instruments, Rockville, MA, USA). Before testing, each 2 mm-diameter disk was cut into two semi-cylindrical microcompression specimens with a custom cutter. The remaining tissue annulus for each plug was frozen and saved for biochemical analyses. Each annulus was sectioned axially into three tissue slices of equal thickness and FCD determined using the DMMB dye-binding assay following the method described by Narmoneva et al. [36].

A confined compression microscopy device was designed for this study, which incorporated a semi-cylindrical confining ring with porous platen at bottom and a semi-cylindrical impermeable stainless steel indenter. The indenter was rigidly connected to a precision miniature load cell (Model 31; Sensotec Inc., Columbus, OH, USA; range 0–150 grams) and then to a differential screw translator (M-R-O Industrial Supplies, Manville, NJ, USA; resolution 1 μm). The tissue sample, with the cross section of tissue depth facing down, was confined compressed with the impermeable indenter, while bathed in NaCl solution + PI contained in an immersion chamber with a glass window at bottom. The custom loading device was mounted onto the motorized stage (ProScan H128 Series; Prior Scientific, Rockland, MA, USA) of an inverted microscope (Olympus IX70; Olympus America, Melville, NY, USA) equipped for transmission and epifluorescence microscopy with a 100 W Xenon arc lamp, a DeltaRam high speed monochromator, a DAPI filter cube, and a Uplan 10 \times objective (Olympus America, Melville, NY, USA). The optical path of the microscope was adjusted through the immersion chamber and the cross section of tissue depth between the platens was focused and visualized. All images were captured such that the image width contained the central region of the cross section. As shown in Fig. 1, the half-cylindrical specimen was first equilibrated in hypertonic saline (2 M NaCl) for 45 minutes. The initial thickness (h_0) was optically determined by moving the indenter until no space could be observed from either side of the specimen (Fig. 2, I). The specimen was then compressed 10% of h_0 (Fig. 2, II) and permitted to relax

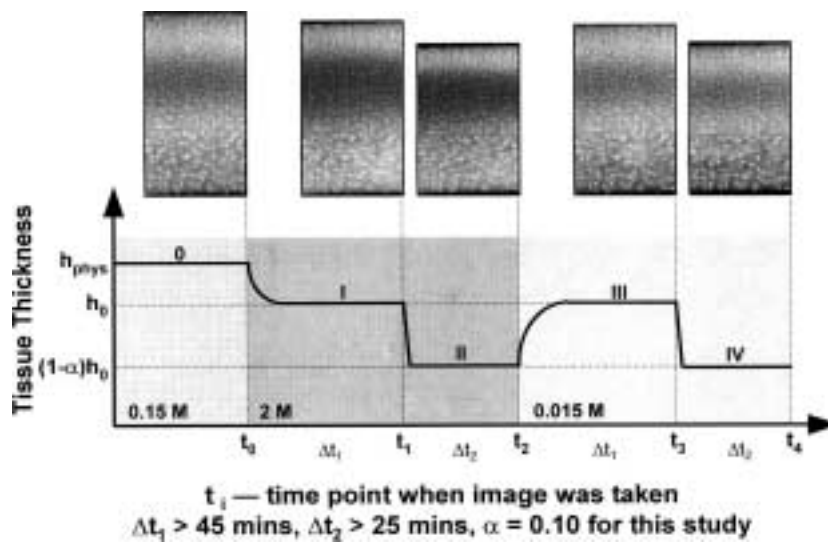


Fig. 2. Experimental protocol for determination of the depth-dependent intrinsic solid matrix stiffness ($H_a(z)$) and intrinsic fixed charge density ($c_0^F(z)$). In the plot of the tissue thickness versus time, h_{phys} is the initial thickness of the tissue specimen in physiological saline (0.15 M NaCl), h_0 is the initial thickness of the tissue specimen in 2M NaCl and $(1 - \alpha)h_0$ is the tissue thickness after applied compression.

to equilibrium, and images of the cross section recorded. Next, the distance between the bottom of the confining ring and the indenter was reset to h_0 . The bathing solution was then changed to 0.015 M (Fig. 2, III) and the preceding loading protocol repeated (Fig. 2, IV).

The strain distributions resulting from mechanical and/or osmotic loading were determined automatically using an optimized digital image correlation (DIC) technique and a thin-plate spline smoothing algorithm. By simple manipulation of the common Donnan osmotic equation, we get the expression $\pi = RT(\sqrt{c^{F^2} + 4c^{*2}} - 2c^*)$ [21]. Thus, under extreme hypertonic conditions when $c^* \gg c^F$ (e.g., $c^* = 2$ M), the osmotic pressure in cartilage is negligible. According to Eqs (2) and (5), at equilibrium,

$$\sigma^T = H_a \varepsilon - \pi. \quad (6)$$

Under extreme hypertonic conditions ($c^* = 2$ M), since $\pi \approx 0$, hence measurements of the depth-dependent strain field ($\varepsilon(z)$) in a specimen subjected to a prescribed surface-to-surface clamping strain (Fig. 2, I to II) provides a measure of the inhomogeneity of the intrinsic solid matrix stiffness ($H_a(z)$), i.e.,

$$H_a(z) \simeq \left. \frac{\sigma^T}{\varepsilon(z)} \right|_{c^*=2 \text{ M}}. \quad (7)$$

If this sample, subjected to the same clamping strain, is then exposed to an isotonic/hypotonic salt environment (Fig. 2, II to IV), its osmotic pressure rises according to the local distribution of effective FCD; if this distribution is inhomogeneous, the depth-dependent strain will change accordingly. Thus, a measure of the change in depth-dependent strain ($\varepsilon(z)$) between hypertonic and hypotonic conditions (e.g., 0.015 M), coupled with knowledge of the clamping stress, can produce a measure of the osmotic pressure distribution ($\pi(z)$), i.e.,

$$\pi(z) = H_a(z) \cdot \varepsilon(z)|_{c^*=0.015 \text{ M}} - \sigma^T|_{c^*=0.015 \text{ M}}, \quad (8)$$

from which the effective FCD can be determined as

$$c^F|_{c^*=0.015 \text{ M}} = \frac{\pi}{RT} \sqrt{1 + \frac{4c^*RT}{\pi}} \Big|_{c^*=0.015 \text{ M}}. \quad (9)$$

The intrinsic FCD (c_0^F) can thus be obtained from the conservation equation of fixed charges (Eq. (1)), given the resultant strains ($\varepsilon(z)$) due to the mechanical and osmotic loading (Fig. 2, 0 to IV).

3. Results

Compressive loading (10% of h_0) under hypertonic conditions (Fig. 2, from I to II) resulted in a nonlinear axial displacement distribution within the tissue along the axial (or depth) direction. The displacement field for a representative cartilage specimen is shown in Fig. 3(a). These axial displacements exhibit no significant variation along the radial direction ($p > 0.9$); the optimized DIC also measured an average lateral displacement of $0.14 \pm 0.16 \mu\text{m}$, which is on the order of the system errors introduced by the image acquisition. Together, these data demonstrate a perfect confinement of the specimen within the

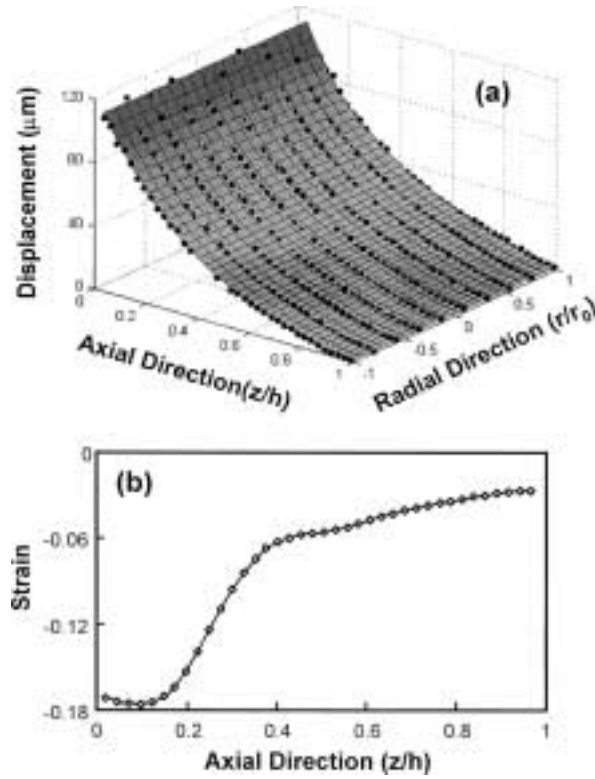


Fig. 3. (a) The resultant displacement field arising from compressive loading in hypertonic (2M NaCl) solution (Fig. 2, I to II). The shaded surface represents the thin-plate smooth fitting spline of the displacement field. (b) Plot of the depth-dependent strain distribution obtained from differentiation of the thin-plate smooth fitting spline.

confining ring. The shaded surface in Fig. 3(a) represents the thin-plate smooth fitting spline of the measured axial displacement fields ($R^2 = 0.99$). Strain analysis performed by differentiating the smoothed surface revealed an inhomogeneous strain distribution along the axial direction, with the magnitude decreasing from the surface layer to the deep layer (Fig. 3(b)). Since the osmotic effects are negligible under the extreme hypertonic condition, the intrinsic matrix stiffness ($H_a(z)$) for the specimen in Fig. 3(a) can be determined from Eq. (7) (Fig. 5(a)).

Under the same clamping strain (10% of h_0), the introduction of osmotic loading via change of bathing solution concentration from 2 M to 0.015 M (Fig. 2, II to IV) yielded a non-uniform displacement field within the same specimen (Fig. 4(a)). Again, no significant variation of the axial displacement was observed along the radial direction ($p > 0.85$). The resultant strain distribution (Fig. 4(b)) was determined from the thin-plate smooth fitting spline of the displacement data ($R^2 = 0.92$). The osmotic effects are no longer negligible under this hypotonic condition; from Eq. (6), the surface traction on the specimen surface arises from both the osmotic pressure and the elastic stress of the solid matrix. With knowledge of the intrinsic matrix stiffness $H_a(z)$ (Fig. 5(a)) and the measured osmotic strain distribution (Fig. 4(b)), the depth-dependent osmotic pressure π was determined (Fig. 4(c)). By further noticing that the osmotic pressure can be expressed as a function of the effective FCD of the tissue as well as the bathing concentration, a depth-dependent effective FCD ($c^F(z)$) can be determined from the osmotic pressure distribution. Furthermore, the intrinsic FCD ($c_0^F(z)$) for the same specimen was determined using Eq. (1) and is plotted in Fig. 5(b).

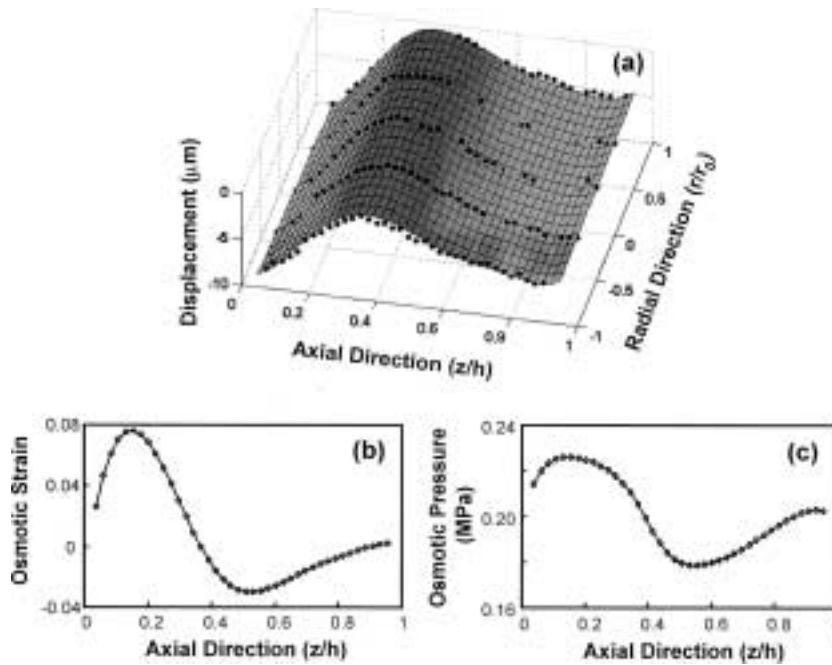


Fig. 4. (a) The resultant displacement field arising from osmotic loading (Fig. 2, II to IV). The shaded surface represents the thin-plate smooth fitting spline of the displacement field. (b) Plot of the depth-dependent strain distribution obtained from differentiation of the thin-plate smooth fitting spline. (c) Plot of the depth-dependent osmotic pressure π .

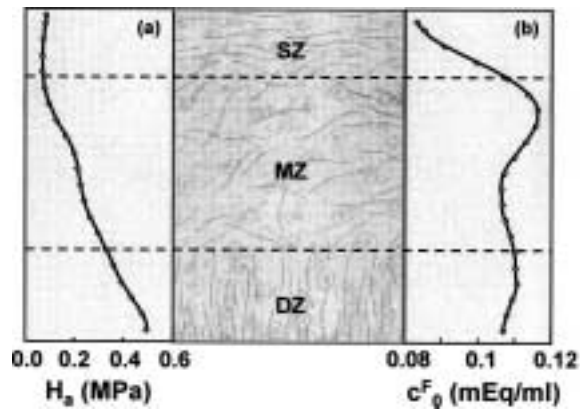


Fig. 5. The depth-dependent intrinsic solid matrix stiffness ($H_a(z)$) and intrinsic fixed charge density ($c_0^F(z)$) determined for a typical young bovine articular cartilage specimen. These properties are incorporated in our theoretical analysis of the tissue behavior under confined compression.

The distributions of intrinsic matrix stiffness ($H_a(z)$) and FCD ($c_0^F(z)$) (Fig. 5) were then incorporated into the triphasic model to analyze the transient environment of chondrocytes within a cartilage explant under confined compression with the articular surface against the porous loading platen. It is noted that for the purpose of comparison, an average intrinsic FCD and an “equivalent” constant intrinsic

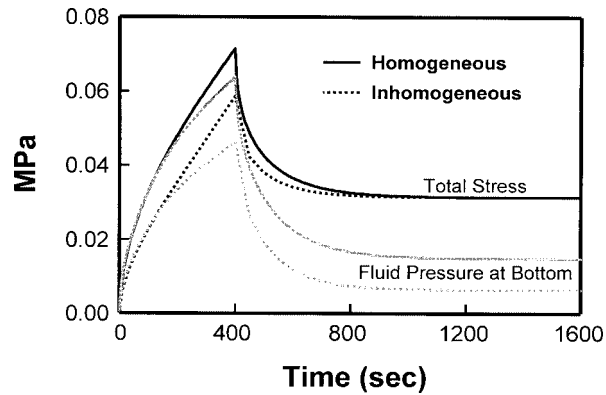


Fig. 6. The stress relaxation response of cartilage specimens with homogeneous and inhomogeneous intrinsic solid matrix stiffness and intrinsic fixed charge density. The fluid pressure determined at the bottom of the specimen ($z = h$) is also depicted to show the degree of load support by the fluid phase.

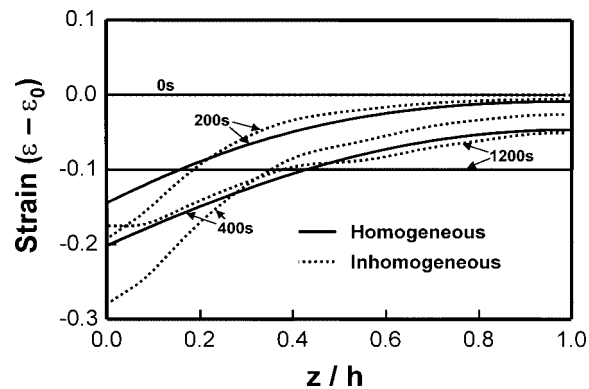


Fig. 7. Plot of the spatial distribution and temporal development of strain for the homogeneous and inhomogeneous tissue subjected to stress relaxation in confined compression. $z = 0$ corresponds to the articular surface.

insic matrix stiffness³ were used for a homogeneous model in the following results. Comparison of the stress–relaxation curves for the homogeneous and inhomogeneous tissues clearly shows distinct differences in the transient development of stress before equilibrium is reached at 1200 seconds (Fig. 6). The homogeneous model predicts a greater peak stress and lengthier relaxation phase. For both models, the loading-induced tissue deformation proceeds from the surface zone to the deep zone, with the strain eventually being distributed equally throughout the tissue depth for the homogeneous case (Fig. 7). It should be emphasized that during the transient loading phase (i.e., before equilibrium is reached) the peak strains within the tissue for each case can exceed the nominally applied 10% surface-to-surface strain. This result is indicative of the applied loading condition (1D loading with a permeable platen). The inhomogeneity of the tissue amplifies the conditions established by this applied loading condition. Although the stress relaxation test is performed with the zero external applied loading condition as the reference, there exists an initial prestress due to the osmotic pressure within the proteoglycan–collagen

³The “equivalence” between the homogeneous tissue and inhomogeneous tissue is defined such that both tissues, which have the same values for all the parameters except $c_0^F(z)$ and $H_a(z)$, should achieve the same equilibrium stress in the stress–relaxation test.

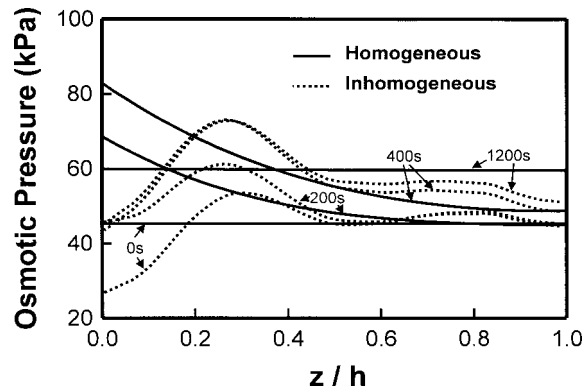


Fig. 8. Plot of the spatial distribution and temporal development of osmotic pressure for the homogeneous and inhomogeneous tissue subjected to stress relaxation in confined compression. $z = 0$ corresponds to the articular surface.

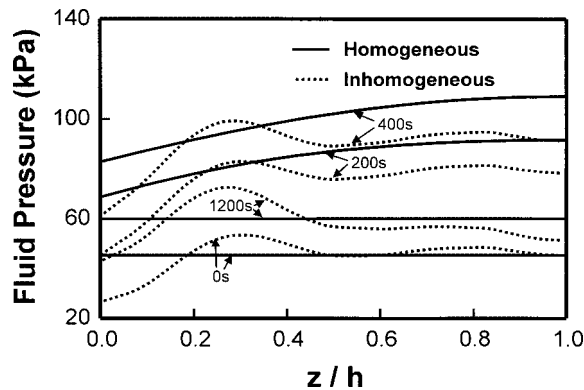


Fig. 9. Plot of the spatial distribution and temporal development of fluid pressure for the homogeneous and inhomogeneous tissue subjected to stress relaxation in confined compression. At $t = 0$ and at equilibrium, the fluid pressure is equal to the osmotic pressure (Fig. 8). $z = 0$ corresponds to the articular surface.

network of the tissue (Fig. 8). This prestress generates an initial free-swelling strain (ε_0) distribution (constant throughout the depth in the homogeneous case) within the tissue (Fig. 7).

The FCD and the tissue stiffness govern the osmotic pressure within the tissue. In the case of the homogeneous tissue, the strain distribution alone accounts for the development of non-uniform osmotic pressure in the tissue during the transient phase. Conversely, the existence of an intrinsic inhomogeneous FCD gives rise to an initial non-uniform osmotic pressure (and initial matrix strain) which is then modulated by the subsequent loading-induced matrix strain. From Figs 7 and 8, the spatial and temporal development of solid matrix deformation and osmotic pressure are directly related, with the peak osmotic pressure (and peak compressive matrix deformation) in the tissue corresponding to the surface zone ($z = 0$) at time 400 seconds. Accordingly, the osmotic pressure distribution parallels the uniform strain distribution in the tissue at equilibrium for the homogeneous case.

The load during the stress relaxation test is partitioned between the solid and fluid phases of the tissue, manifested as matrix stress and fluid pressure. In the triphasic model, the fluid pressure derives from both the hydrodynamic fluid pressure and the osmotic pressure. Accordingly, from Fig. 9, the fluid pressure is equal to the osmotic pressure at $t = 0$ and at the equilibrium condition (1200 sec) when there is no longer fluid exudation from the tissue. At equilibrium, the measurable load (e.g., calculated total stress)

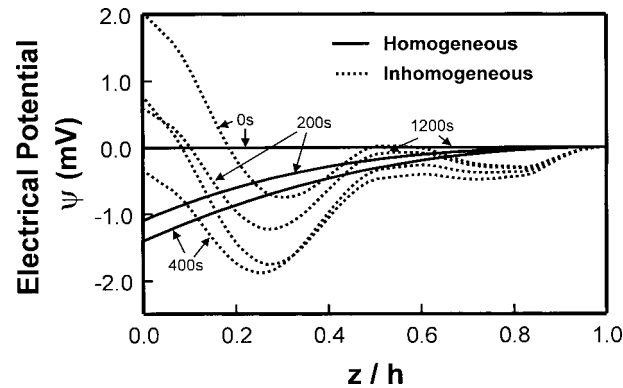


Fig. 10. Plot of the spatial distribution and temporal development of electrical potential for the homogeneous and inhomogeneous tissue subjected to stress relaxation in confined compression. $z = 0$ corresponds to the articular surface.

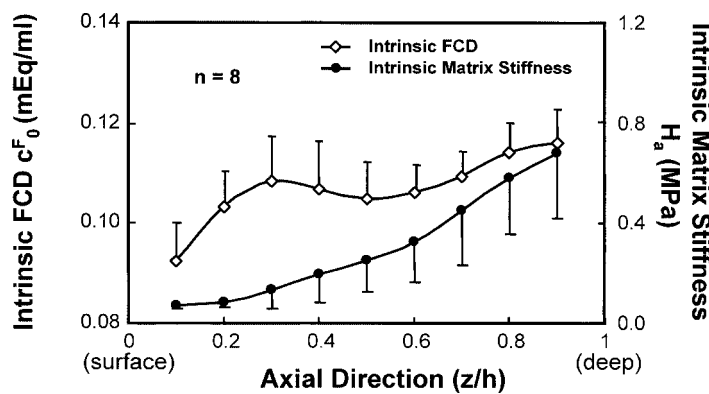


Fig. 11. A summary of the depth-dependent intrinsic solid matrix stiffness ($H_a(z)$) and intrinsic fixed charge density ($c_0^F(z)$) for 8 young bovine articular cartilage specimens determined using the non-invasive methodology described in the text and the experimental protocol depicted in Fig. 2.

reflects the change in osmotic pressure and solid matrix stress. During the loading period, there can be significant load support by the fluid pressure (Fig. 6). This fluid support has been proposed to contribute significantly to cartilage's load-bearing and lubrication capacity [3,29,50].

The electrical potential (Fig. 10) in the homogeneous tissue is zero at $t = 0$ and at $t = 1200$ seconds. This results from the uniform distribution of FCD within the tissue before loading and at equilibrium. In contrast, electrical potential gradients exist in the inhomogeneous case during the entire stress relaxation response due to the intrinsic inhomogeneous FCD distribution. At $t = 0$ and equilibrium, the distribution of the electrical potential resembles that for the FCD distribution within the inhomogeneous tissue. From Fig. 10, there is a sign change in the electrical potential inside the inhomogeneous tissue that is not observed for the homogeneous tissue.

Although the theoretical analysis of the spatial and time-varying mechanical and electrochemical events (Figs 6–10) was performed using parameters derived from a single cartilage specimen, it should be noted that its inhomogeneous properties are representative of seven other samples derived from 4 young bovine carpalometacarpal joints. We summarize the intrinsic solid matrix stiffness and intrinsic FCD from all 8 cartilage specimens in Fig. 11. For qualitative comparison, the mean FCD determined from biochemical analyses of the top slices (which contains the surface zone) was 0.098 ± 0.016 mEq/ml, the

middle slices was 0.112 ± 0.019 mEq/ml and the bottom slices (which contains the deep zone) was 0.132 ± 0.063 mEq/ml.

4. Discussion

While surface-to-surface measurements (such as the confined aggregate modulus or surface-to-surface applied strain) provide bulk properties or bulk characterization of a tissue, they provide only indirect insights to the internal behavior of the tissue or the development of spatial and temporal gradients of strain, pressure, osmotic pressure and electric potentials. Since cells may sense change as well as stimulus magnitude (e.g., [11]), spatial and time-varying fields or gradients of stimuli may be important in chondrocyte mechanotransduction and related changes to cell biosynthetic and catabolic activities [30]. From our analysis of a homogeneous tissue subjected to the simple loading case of uniaxial confined compression, one can quickly gain an appreciation for the complexity of the environment within the tissue during loading. When a more accurate description of the tissue properties (inhomogeneous intrinsic tissue stiffness and FCD) is incorporated into the analysis, the variation of the cell environment within the tissue becomes even more pronounced.

Using confocal microscopy, Guilak and co-workers [14] demonstrated depth-varying cell deformation in loaded explants, being greatest in the superficial zone. Consistent with this finding is that of a depth-dependent aggregate modulus reported in the literature [42,43,46]. Our measurements also reveal a depth-dependent aggregate modulus, as well as a depth-dependent FCD [55,58] determined through mechanical and osmotic loading. The current investigation represents the first effort to incorporate experimental measurements of inhomogeneous aggregate modulus and FCD into a theoretical analysis of articular cartilage loading behavior. While our experiments can permit determination of the FCD, osmotic pressure, hydrostatic pressure and strain at equilibrium, we are unable to currently apply our technique to the transient phase of the stress-relaxation response. However, with constitutive modeling we can predict the time-varying environment within the tissue.

The novel non-invasive methodology used to determine the intrinsic tissue stiffness and the intrinsic FCD for the same specimen utilized a custom loading device, digital video microscopy, optimized digital image correlation technique and application of the familiar equations for Donnan osmotic pressure [55,58]. The technique reports FCD values that are similar to those reported using conventional techniques for determination of FCD [25,26] and are in qualitative agreement with our own biochemistry results. Thus, our methodology appears to represent an alternative means for determination of FCD in soft hydrated tissues without requiring excessive tissue sectioning. Efforts to further validate this non-invasive methodology are currently underway. Assumptions in the study included the use of a linear stress/strain law to describe the deformation behavior of the solid matrix and ideal Donnan behavior. In the future, non-ideal Donnan behavior may be incorporated, including deviations of the osmotic coefficient from unity at low salt concentrations [6], and configurational entropy effects which produce an osmotic pressure above and beyond Donnan electrostatic interactions [9,20,54]; similarly, other tissue inhomogeneities can be incorporated, theoretically or through measured parameters, into the theoretical framework adopted in this study. Tissue anisotropy [8,9], tension-compression nonlinearity [16,49] and intrinsic viscoelasticity [16,51] are other properties that can be introduced as well.

Coupled with biological assays of cell-scale chondrocyte biosynthesis [38,60,61] and real-time fluorescence probes of cellular activities [40], there is a great potential in the future to study chondrocyte mechanotransduction *in situ* with a new level of specificity. With a better prediction of the chondrocyte

environment *in situ*, we may begin to elucidate the mechanisms that underlie normal cartilage maintenance as well as the etiology of osteoarthritis [33]. Similarly, an understanding of the changes to the tissue inhomogeneity that accompany aging and disease may provide clues to the initiation and progression of joint degeneration [2,4,10,41,44,45]. It may also be used to assess the development of inhomogeneity in tissue engineered cartilage constructs, and to explore means of prescribing tissue inhomogeneity in growing tissues via modulation of the physical environment (e.g., loading, chemical mediators etc.) in custom bioreactors.

Acknowledgements

This study was supported by the National Institute of Arthritis and Musculoskeletal and Skin Diseases (NIAMS) of the National Institutes of Health (AR 46568, AR 41913, AR 46532 and AR 45832). The authors also would like to thank Ms. Nadeen O. Chahine for help in the experiments.

References

- [1] S. Akizuki, V.C. Mow, F. Muller, J.C. Pita, D.S. Howell and D.H. Manicourt, Tensile properties of human knee joint cartilage: I. Influence of ionic concentrations, weight bearing and fibrillation on the tensile modulus, *J. Orthop. Res.* **4** (1986), 379–392.
- [2] C.G. Armstrong and V.C. Mow, Variations in the intrinsic mechanical properties of human articular cartilage with age degeneration and water content, *J. Bone Jt. Surg.* **64A** (1982), 88–94.
- [3] G.A. Ateshian, H. Wang and W.M. Lai, The role of interstitial fluid pressurization and surface porosities on the boundary friction of articular cartilage, *J. Tribology* **120** (1998), 241–248.
- [4] J.A. Buckwalter, K.E. Kuettner and E.J.-M. Thonar, Age-related changes in articular proteoglycans: Electron microscopic studies, *J. Orthop. Res.* **3** (1985), 251–257.
- [5] M.D. Buschmann, Y.A. Gluzband, A.J. Grodzinsky and E.B. Hunziker, Mechanical compression modulates matrix biosynthesis in chondrocyte/agarose cultures, *J. Cell Sci.* **108** (1995), 1497–1508.
- [6] M.D. Buschmann and A.J. Grodzinsky, A molecular model of proteoglycan-associated electrostatic forces in cartilage mechanics, *J. Biomech. Eng.* **117** (1995), 179–192.
- [7] P.-H.G. Chao, R. Roy, R.L. Mauck, W. Liu, W.B. Valhmu and C.T. Hung, Chondrocyte translocation response to direct current electric fields, *J. Biomech. Eng.* **122** (2000).
- [8] B. Cohen, W.M. Lai, G.S. Chorney, H.M. Dick and V.C. Mow, Unconfined compression of transversely-isotropic biphasic tissue, *Adv. Bioengng. Trans. ASME BED-19* (1992), 187–190.
- [9] S. Ehrlich, N. Wolff, R. Schneiderman, A. Maroudas, K.H. Parker and C.P. Winlove, The osmotic pressure of chondroitin sulphate solutions: Experimental measurements and theoretical analysis, *Biorheology* **35:6** (1998), 383–397.
- [10] D.R. Eyre, I.R. Dickson and K.P. Van Ness, Collagen cross-linking in human bone and articular cartilage. Age related changes in the content of matrix hydroxypyridinium residues, *Biochem. J.* **252** (1988), 495–500.
- [11] J. Frangos, T. Huang and C.B. Clark, Steady shear and step changes in shear stimulate endothelium via independent mechanisms – superposition of transient and sustained nitric oxide production, *Biochem. Biophys. Res. Commun.* **224** (1996), 660–665.
- [12] E.H. Frank and A.J. Grodzinsky, Cartilage electromechanics-II. A continuum model of cartilage electrokinetics and correlation with experiments, *J. Biomechanics* **20** (1987), 629–639.
- [13] W.Y. Gu, W.M. Lai and V.C. Mow, A mixture theory for charged-hydrated soft tissues containing multi-electrolytes: passive transport and swelling behaviors, *J. Biomech. Eng.* **120** (1997), 169–180.
- [14] F. Guilak, A. Ratcliffe and V.C. Mow, Chondrocyte deformation and local tissue strain in articular cartilage: a confocal microscopy study, *J. Orthop. Res.* **13** (1995), 410–422.
- [15] F. Guilak, H.P. Ting-Beall, W.R. Jones, G.M. Lee and R.M. Hochmuth, Mechanical properties of chondrocytes and chondrons, *Adv. Bioengng. Trans. ASME BED-33* (1996), 253–254.
- [16] C.-Y. Huang, A. Stankiewicz, G.A. Ateshian, E.L. Flatow, L.U. Bigliani and V.C. Mow, Anisotropy, inhomogeneity and tension–compression nonlinearity of human glenohumeral cartilage in finite deformation, *Trans. Orthop. Res. Soc.* **24** (1999), 95.

- [17] C.T. Hung, D. Henshaw, C.C.-B. Wang, R.L. Mauck, F. Raia, G. Palmer, V.C. Mow, A. Ratcliffe and W.B. Valhmu, Mitogen-activated protein kinase signaling in bovine articular chondrocytes in response to fluid flow does not require calcium mobilization, *J. Biomechanics* **33** (2000), 73–80.
- [18] J.S. Jurvelin, M.D. Buschmann and E.B. Hunziker, Optical and mechanical determination of Poisson's ratio of adult bovine humeral articular cartilage, *J. Biomechanics* **30** (1997), 235–241.
- [19] G.E. Kempson, Mechanical properties of articular cartilage, in: *Adult Articular Cartilage*, M.A.R. Freeman, ed., Pitman Medical, Kent, England, 1979, pp. 333–414.
- [20] I.S. Kovach, The importance of polysaccharide configurational entropy in determining the osmotic swelling pressure of concentrated proteoglycan solution and the bulk compressive modulus of articular cartilage, *Biophys. Chem.* **53** (1995), 181–187.
- [21] W.M. Lai, J.S. Hou and V.C. Mow, A triphasic theory for the swelling and deformational behaviors of articular cartilage, *J. Biomech. Eng.* **113** (1991), 245–258.
- [22] M.J. Lammi, R. Inkinen, J.J. Parkkinen, T. Jakkinen, M. Jortikka, L.O. Nelimarkka, H.T. Jarvelainen and M.I. Tammi, Expression of reduced amounts of structurally altered aggrecan in articular cartilage chondrocytes exposed to high hydrostatic pressure, *Biochem. J.* **304** (1994), 723–730.
- [23] D.A. Lee and D.L. Bader, Compressive strains at physiological frequencies influence the metabolism of chondrocytes seeded in agarose, *J. Orthop. Res.* **15** (1997), 181–188.
- [24] A.I. Maroudas, Balance between swelling pressure and collagen tension in normal and degenerate cartilage, *Nature* **260** (1976), 808–809.
- [25] A.I. Maroudas, H. Muir and J. Wingham, The correlation of fixed negative charge with glycosaminoglycan content of human articular cartilage, *Biochim. Biophys. Acta* **177** (1969), 492–500.
- [26] A.I. Maroudas, Physicochemical properties of articular cartilage, in: *Adult Articular Cartilage*, M.A.R. Freeman, ed., Pitman Medical, Kent, UK, 1979, pp. 215–290.
- [27] I. Martin, B. Obradovic, L.E. Freed and G. Vunjak-Novakovic, Method for quantitative analysis of glycosaminoglycan distribution in cultured natural and engineered cartilage, *Ann. Biomed. Eng.* **27** (1999), 656–662.
- [28] R.L. Mauck, M.A. Soltz, C.C.-B. Wang, D.D. Wong, P.-H.G. Chao, W.B. Valhmu, C.T. Hung and G.A. Ateshian, Functional tissue engineering of articular cartilage through dynamic loading of chondrocyte-seeded agarose gels, *J. Biomech. Eng.* **122** (2000), 252–260.
- [29] V.C. Mow and G.A. Ateshian, Lubrication and wear of diarthrodial joints, in: *Basic Orthopaedic Biomechanics*, V.C. Mow and W.C. Hayes, eds, 1997, Lippincott-Raven, Philadelphia, pp. 273–315.
- [30] V.C. Mow, N.M. Bachrach, L.A. Setton and F. Guilak, Stress, strain, pressure and flow fields in articular cartilage and chondrocytes, in: *Cell Mechanics and Cellular Engineering*, V.C. Mow, F. Guilak, R. Tran-Son-Tay and R.M. Hochmuth, eds, 1994, Springer-Verlag, New York, pp. 345–379.
- [31] V.C. Mow, S.C. Kuei, W.M. Lai and C.G. Armstrong, Biphasic creep and stress relaxation of articular cartilage in compression: theory and experiments, *J. Biomech. Eng.* **102** (1980), 73–84.
- [32] V.C. Mow and A. Ratcliffe, Structure and function of articular cartilage and meniscus, in: *Basic Orthopaedic Biomechanics*, V.C. Mow and W.C. Hayes, eds, 1997, Lippincott-Raven, Philadelphia, pp. 113–177.
- [33] V.C. Mow, C.C.-B. Wang and C.T. Hung, The extracellular matrix, interstitial fluid and ions as a mechanical signal transducer in articular cartilage, *Osteoarthritis Cartilage* **7** (1999), 41–59.
- [34] V.C. Mow and C.C.-B. Wang, Some bioengineering considerations for tissue engineering of articular cartilage, *Clin. Orthop.* **367** Suppl. (1999), S204–S223.
- [35] D.A. Narmoneva and L.A. Setton, Measurement of nonuniform swelling strains in full-thickness articular cartilage, *Trans. Orthop. Res. Soc.* **22** (1997), 81.
- [36] D.A. Narmoneva, J.Y. Wang and L.A. Setton, Nonuniform swelling-induced residual strains in articular cartilage, *J. Biomechanics* **32** (1999), 401–408.
- [37] J.J. Parkkinen, J. Ikonen, M.J. Lammi, J. Laakkonen, M. Tammi and H.J. Helminen, Effects of cyclic hydrostatic pressure on proteoglycan synthesis in cultured chondrocytes and articular cartilage explants, *Arch. Biochem. Biophys.* **300** (1993), 458–465.
- [38] T. Quinn, A. Grodzinsky, M. Buschmann, Y. Kim and E. Hunziker, Mechanical compression alters proteoglycan deposition and matrix deformation around individual cells in cartilage explants, *J. Cell Sci.* **111** (1998), 573–583.
- [39] P.M. Ragan, V.I. Chin, H.H. Hung, K. Masuda, E.J. Thonar, E.C. Arner, A.J. Grodzinsky and J.D. Sandy, Chondrocyte extracellular matrix synthesis and turnover are influenced by static compression in a new alginate disk culture system, *Arch. Biochem. Biophys.* **383** (2000), 256–264.
- [40] S. Roberts, M. Knight, D. Lee and D. Bader, Mechanical compression influences intracellular Ca^{2+} signaling in chondrocytes seeded in agarose constructs, *J. Appl. Physiol.* **90** (2001), 1385–1391.
- [41] V. Roth and V.C. Mow, The intrinsic tensile behavior of the matrix of bovine articular cartilage and its variation with age, *J. Bone Jt. Surg.* **62A** (1980), 1102–1117.

- [42] R.M. Schinagl, D. Gurkis, C.C. Chen and R.L.-Y. Sah, Depth-dependent confined compression modulus of full-thickness bovine articular cartilage, *J. Orthop. Res.* **15** (1997), 499–506.
- [43] R.M. Schinagl, M.K. Ting, J.H. Price and R.L. Sah, Video microscopy to quantitate the inhomogeneous equilibrium strain within articular cartilage during confined compression, *Ann. Biomed. Eng.* **24** (1996), 500–512.
- [44] L.A. Setton, D.M. Elliot and V.C. Mow, Altered mechanics of cartilage with osteoarthritis: human osteoarthritis and an experimental model of joint degeneration, *Osteoarthritis Cartilage* **7** (1999), 2–14.
- [45] L.A. Setton, V.C. Mow, F.J. Muller, J.C. Pita and D.S. Howell, Mechanical behavior and biochemical composition of canine knee cartilage following periods of joint disuse and disuse with remobilization, *Osteoarthritis Cartilage* **5** (1997), 1–16.
- [46] D. Shin, J.-H. Lin and K. Athanasiou, Microindentation of the individual layers of articular cartilage, *Adv. Bioengng. Trans. ASME BED-36* (1997), 155–156.
- [47] R.L. Smith, B.S. Donlon, M.K. Gupta, M. Mohtai, P. Das, D.R. Carter, J. Cooke, G. Gibbons, N. Hutchinson and D.J. Schurman, Effects of fluid-induced shear on articular chondrocyte morphology and metabolism *in vitro*, *J. Orthop. Res.* **13** (1996), 824–831.
- [48] R.L. Smith, S.F. Rusk, B.E. Ellison, P. Wessells, K. Tsuchiya, D.R. Carter, W.E. Caler, L.J. Sandell and D.J. Schurman, In vitro stimulation of articular chondrocyte mRNA and extracellular matrix synthesis by hydrostatic pressure, *J. Orthop. Res.* **14** (1996), 53–60.
- [49] M.A. Soltz and G.A. Ateshian, A conewise linear elasticity mixture model for the analysis of tension–compression non-linearity in articular cartilage, *J. Biomech. Eng.* **122** (2000), 576–586.
- [50] M.A. Soltz and G.A. Ateshian, Experimental verification and theoretical prediction of cartilage interstitial fluid pressurization at an impermeable contact interface in confined compression, *J. Biomechanics* **31** (1998), 927–934.
- [51] J.K. Suh and S. Bai, Finite element formulation of biphasic poroviscoelastic model for articular cartilage, *J. Biomech. Eng.* **120** (1998), 195–201.
- [52] D.N. Sun, W.Y. Gu, X.E. Guo, W.M. Lai and V.C. Mow, A mixed finite element formulation of triphasic mechano-electrochemical theory for charged, hydrated biological soft tissues, *Int. J. Numer. Meth. Engng.* **45** (1999), 1375–1402.
- [53] D.N. Sun, W.Y. Gu, X.E. Guo, W.M. Lai and V.C. Mow, The influence of inhomogeneous fixed charge density of cartilage mechano-electrochemical behaviors, *Trans. Orthop. Res. Soc.* **23** (1998), 484.
- [54] J.P.G. Urban, A. Maroudas, M.T. Bayliss and J. Dillon, Swelling pressures of proteoglycans at the concentrations found in cartilaginous tissues, *Biorheology* (1979), 447–464.
- [55] C.C.-B. Wang, X.E. Guo, J.J. Deng, V.C. Mow, G.A. Ateshian and C.T. Hung, A novel non-invasive technique for determining distribution of fixed charge density within articular cartilage, *Trans. Orthop. Res. Soc.* **26** (2001), 129.
- [56] C.C.-B. Wang, C.T. Hung and V.C. Mow, Analysis of the effects of depth-dependent aggregate modulus on articular cartilage stress–relaxation behavior in compression, *J. Biomechanics* **34** (2000), 75–84.
- [57] C.C.-B. Wang and V.C. Mow, Effects of aggregate modulus inhomogeneity on cartilage compressive stress-relaxation behavior, *Adv. Bioengng. Trans. ASME BED-39* (1998), 261–262.
- [58] C.C.-B. Wang, M.A. Soltz, R.L. Mauck, W.B. Valhmu, G.A. Ateshian and C.T. Hung, Comparison of equilibrium axial strain distributions in articular cartilage explants and cell-seeded alginate disks under unconfined compression, *Trans. Orthop. Res. Soc.* **25** (2000), 131.
- [59] M. Wong, M. Ponticello, V. Kovanen and J.S. Jurvelin, Volumetric changes of articular cartilage during stress relaxation in unconfined compression, *J. Biomechanics* **33** (2000), 1049–1054.
- [60] M. Wong, P. Wuethrich, M. Buschmann, P. Egli and E. Hunziker, Chondrocyte biosynthesis correlates with local tissue strain in statically compressed adult articular cartilage, *J. Orthop. Res.* **15** (1997), 189–196.
- [61] M. Wong, P. Wuethrich, P. Egli and E. Hunziker, Zone-specific cell biosynthetic activity in mature bovine articular cartilage: a new method using confocal microscopic stereology and quantitative autoradiography, *J. Orthop. Res.* **14** (1996), 424–432.
- [62] S.L.-Y. Woo, W.H. Akeson and G.F. Jemcott, Measurements of nonhomogeneous directional mechanical properties of articular cartilage in tension, *J. Biomechanics* **9** (1976), 785–791.